Impact damage evaluation in composites with infrared thermography

Carosena Meola[1*], Giovanni M. Carlomagno[1], Valentina Lopresto[2], Giancarlo Caprino[2]

[1]Department of Aerospace Engineering (DIAS), University of Naples Federico II,
Via Claudio, 21, 80125 Napoli, ITALY

[2]Department of Materials and Production Engineering (DIMP), University of Naples Federico II,
Piazzale Tecchio, 80, 80125 Napoli, ITALY

ABSTRACT

The aim of the present paper was mainly to highlight thermal phenomena occurring during low-velocity impact of glass-fibre-reinforced plastic laminates with infrared thermography. Several specimens of $[0_2/90_2]_S$ stacking sequence were prepared from unidirectional E-glass fibres embedded in epoxy matrix. These specimens were impacted from one side at different energy values while the ThermaCam SC3000 infrared camera viewed the opposite side. Each specimen was also non-destructively inspected with lock-in thermography before and after impact to search for both manufacturing defects and the damage occurred during impact. The obtained results supply useful information for the material characterization and for estimation of the damage extension through the thickness and in plane for a given depth.

INTRODUCTION

Fibre reinforced composites offer several advantages over metals, mainly high specific stiffness and strength combined with a significant reduction in weight [1-3]. However, due to their low interlaminar strength, these materials are susceptible to delamination, often resulting in considerable loss in compression strength, and possibly leading to catastrophic failures in-service. Due to the high probability of impact-damaging composite materials during manufacture, service and maintenance, it is very important, on one side, the knowledge of the material behaviour under impact and, on the other side, the possibility to discover the damage in its incipient stage. In this context, a valuable technique is infrared thermography [4-7].

Infrared thermography (IRT) is a non-contact, non-intrusive technique which detects the thermal energy radiated from objects in the infrared band of the electromagnetic spectrum; such energy is then transformed into a temperature map. Indeed, a remote imaging system can be used to monitor the entire life of a product, from manufacturing processes to final disposal as well as parts in service.

During dynamic load, two thermal phenomena may occur: one is the thermo-elastic effect which is reversible; the other one is the thermoplastic effect which is irreversible. In metals, the thermo-elastic limit is generally assumed [8] as an indication for the yielding point. In orthotropic materials, as fibre-reinforced polymers (FRP), where it is not possible a direct relationship between the mean stress and Thermo-elastic Stress Analysis (TSA) data [9], the infrared imaging system has been mainly used for damage evolution assessment [10-11]. Besides, within the thermo-elastic stress analysis, the infrared imaging device has been essentially exploited for mapping temperature variations under cyclic loading. Some preliminary results, which are obtained by monitoring with IRT the thermo-elastic phase associated to low-energy impact load, were recently presented by Meola and Carlomagno [12]. They proved that appropriate choice of the sampling rate makes possible to appraise the cooling down of the material, which takes place in a small time fraction.

[*] Corresponding Author: Dr. Carosena Meola
Department of Aerospace Engineering (DIAS)
University of Naples Federico II
Via Claudio 21, 80125 Napoli, ITALY
e-mail: carmeola@unina.it

In this work, IRT is used as surface thermal mapping when specimens are being impacted and as non destructive evaluation (NDE) technique. Owing to on-line monitoring of the impact, the attention is focused on both the thermo-elastic and thermoplastic phases.

MATERIALS AND TEST PROCEDURE

Several specimens, 100 mm wide and 130 mm long, were cut from a 300 mm x 300 mm E-glass/epoxy laminate, using a diamond saw. This hand lay-up laminate was cured at high temperature under press, following the epoxy resin supplier specifications. The laminate staking sequence was $[0_2,90_2]$s and its overall thickness after curing 2.90 mm.

Specimens were first non-destructively inspected with optical lock-in thermography (OLT), to search for manufacturing defects. The setup for non destructive tests (NDT) is sketched in Fig.1. The used infrared camera is the ThermaCam SC3000 (FLIR Systems), which is equipped with a Stirling cooled Focal Plane Array (FPA) Quantum Well (QWIP) detector working in the Long Wave infrared band 8-9 μm. The sensitivity is 20 mK at ambient temperature, allowing for detection of small temperature variations over the specimen surface. The number of pixels is 320 x 240 at the standard acquisition rate of 60 Hz; a vertically reduced field of view is displayed at the highest frame rate of 900 Hz. In OLT, the infrared camera is equipped with the IRLockIn 4 option and with halogen lamps. With the IRLockIn© software, it is possible to select the measurement parameters (heat modulation function, frequency, and acquisition rate), as well as the image processing method (Fast Fourier, Harmonic Approximation, etc.) and the analysis parameters (number of images, first image in the sequence to be analysed, etc.).

Then, the specimens were impacted at different energy levels, in the range 8 - 24 J, using a modified Charpy pendulum by Metrocom (Fig. 2) equipped with a hemispherical impactor 18 mm in diameter (Fig. 3). The energy levels were set by suitably adjusting the falling height. Specimens were hold from the shorter sides, while were free to move along the other two longer sides. The thermal phenomena, which occur during impact, were monitored by viewing the surface opposite to the tup-material contact point with the infrared camera (Fig. 2). Thermal images were acquired in time sequence at 300, or 900 Hz. Indeed, the temperature variations, which are connected to the thermo-elastic effect, occur during very short times (fractions of seconds), and thus, their visualization can be performed only at high frame rates. Each impacted specimen was again inspected with lock-in thermography.

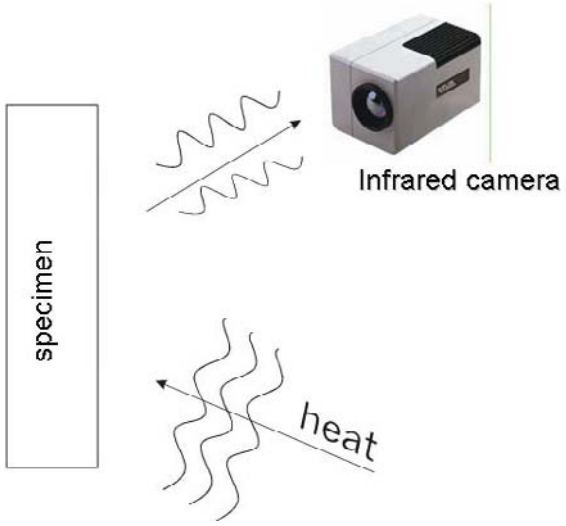

Fig. 1 Setup for non-destructive tests with optical Lock-in thermography

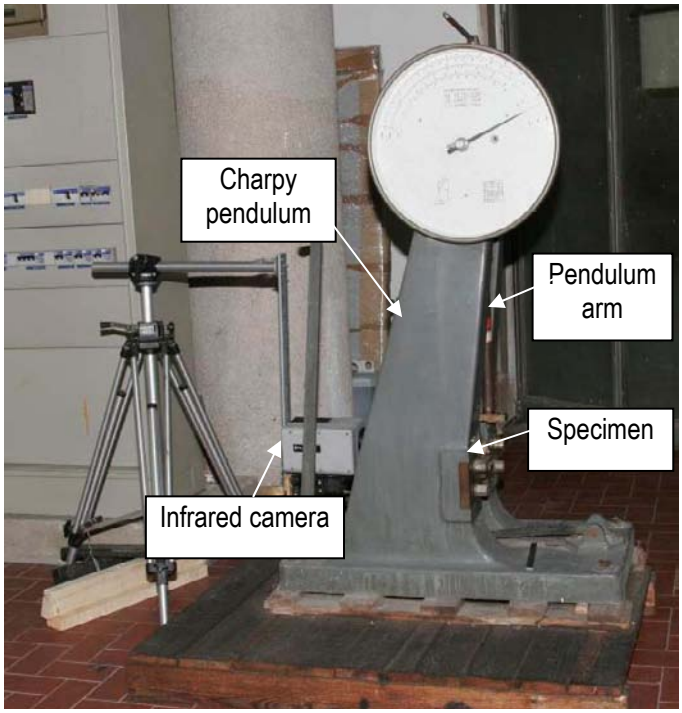

Fig. 2 Experimental set up for monitoring of impacts

Fig. 3 Picture of the impactor

RESULTS AND DISCUSSION

On-line impact monitoring

During impact, the kinetic energy passes from the tup to the target; then, it is in part transformed into elastic energy and in part dissipated through failures, vibrations, or friction. Within a perfect elastic impact, the energy is returned to the impactor, which rebounds recovering the initial height. In Fig. 4, the returned energy (evaluated through the tup rebound height) is plotted against the impact energy. For elastic conditions, all the experimental points fall on the 45° straight line, as the impact energy raises an even more large portion of energy (absorbed energy) is dissipated. Since most of the dissipated energy is converted into heat, the detection of the heat generation loci is important for the comprehension of failure modes; to this extent, the use of infrared thermography is essential.

Thermal images are taken in time-sequence starting just before the impact and ending some time after to include time-dependent thermal phenomena. To better account for the thermal behaviour, the first image (t = 0) of the sequence i.e., the specimen surface (ambient) temperature before impact is subtracted to each subsequent image so as to generate a map of temperature difference ΔT:

$$\Delta T = T(i, j, t) - T(i, j, 0) \qquad (1)$$

i and j representing lines and columns of the surface temperature map. Therefore, a sequence of ΔT images is created.

Several ΔT images taken at different time instants throughout the impact of two specimens impacted at 10 J and 19 J are respectively shown in Figs. 5 and 6. In particular, the images of Fig. 5 belong to a sequence acquired at the fastest acquisition rate, i.e. 900 Hz. Due to the ΔT definition, it is possible to see that the specimen surface displays an overall uniform ΔT = 0 distribution before impact (Fig. 5a). At the impact, the specimen experiences a sudden cooling down (darker zones in figure) because of the elastic material expansion; such a cooling down lasts for few milliseconds. In the meantime, a central hot spot appears (Fig.

5d) being due to the dissipation effect which opposes the reversible elastic phase, with permanent damage growth. Of course, acquisition at 900 Hz allows for monitoring of the elastic phase, but, due to the reduced field of view (only 16 horizontal lines), does not supply reliable information about the vertical extension of the damaged zone.

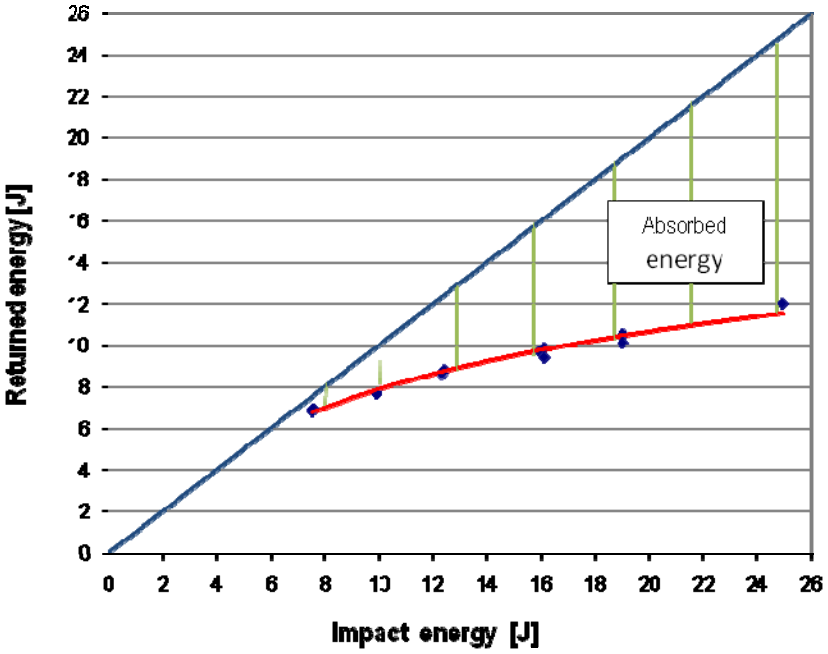

Fig. 4 Impact energy diagram

Even if the duration of the thermo-plastic phase is not much longer of the elastic one its thermal evolution is slower because of the energy dissipation and thus, it is better accounted for through acquisition of images at 300 Hz. In fact, the ΔT images reported in Fig. 6, which belong to a sequence taken at 300 Hz, are composed of 48 horizontal lines (three times those obtained with frame rate of 900 Hz) and then allow for visualization of the whole damaged area. Adversely, as shown in Fig. 6 at 300 Hz, it is not possible to completely distinguish the thermo-elastic phenomena. In fact, the first image that is possible to take at the impact (Fig. 6b) displays cold and hot zones mixed together, which include, at the same time, end of the elastic phase and beginning of the plastic one. In the following image, at 0.0066 s (Fig. 6c), practically only hot spots are evident. Such hot spots grow with time and group to form the warmer zone (Fig. 6d), which witnesses for the permanent damage occurred in the specimen; this is reached after about 0.87 s.

The sequences of images, acquired during impact, were successively analysed to search for a probable correspondence between the damage occurred in the material and the temperature variations displayed on its surface. As can be seen from the images, which are reported in Figs. 5 and 6, the cooling down (dark zones) affects a wide surface with minima close to the impacted zone. Instead, the heating up (lighter colour) starts as localized points (only one or more) where delamination and/or fibre breakage has taken place.

Minima (negative values with respect to the initial ambient temperature) and maxima ΔT values were extracted from each image sequence for the different test conditions. Minima and maxima ΔT, which were evaluated over the surface of a specimen impacted at 12.3 J, are plotted against time in Fig. 7 (a, b). The minimum, which corresponds to the maximum material extension, is attained at the impact instant; after that, the temperature raises towards $\Delta T = 0$ (Fig. 7a) while a secondary minimum is displayed about 0.02 s. The latter is most probably due to a rebound effect. The maximum ΔT is reached after about 0.005 s, it lasts till about 0.02 s and then it decreases slowly towards the ambient temperature.

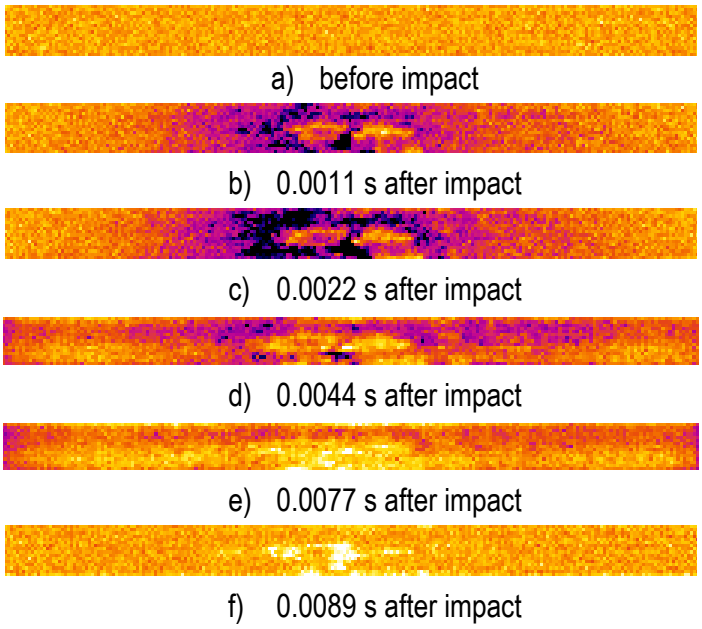

Fig. 5 Images in time sequence (900 Hz) while the specimen is being impacted at 10 J

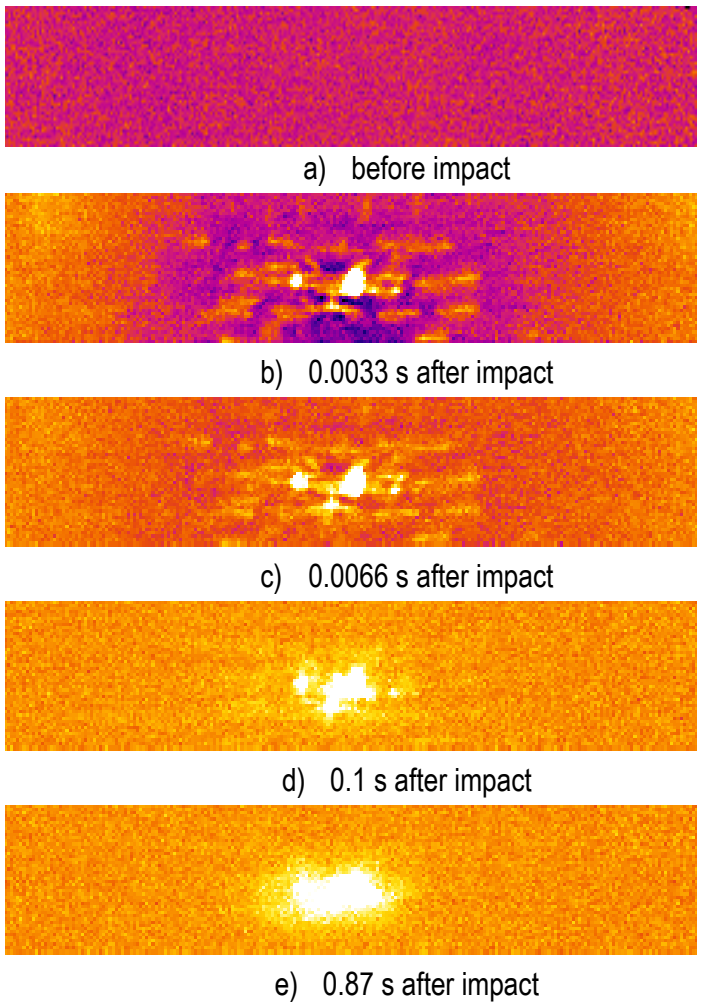

Fig. 6 Images in time sequence (300 Hz) while the specimen is being impacted at 19 J

The warmer area, or better the surface of the specimen which is characterized by temperature raising, is named A_w; such area is measured over each image for all the tested conditions. The distribution of A_w with time for impact energies of 19 and 15.9 J is shown in Fig. 8. As can be seen, A_w increases with increasing the impact energy. For each energy level A_w increases quickly till about 0.3-0.4 s, and then it remains almost constant with small fluctuations around the average value. Indeed, the final A_w value matches the damaged area occurred during impact; the latter is detected through both non destructive inspection after impact and visual inspection, which is possible thanks to the translucent appearance of the panels.

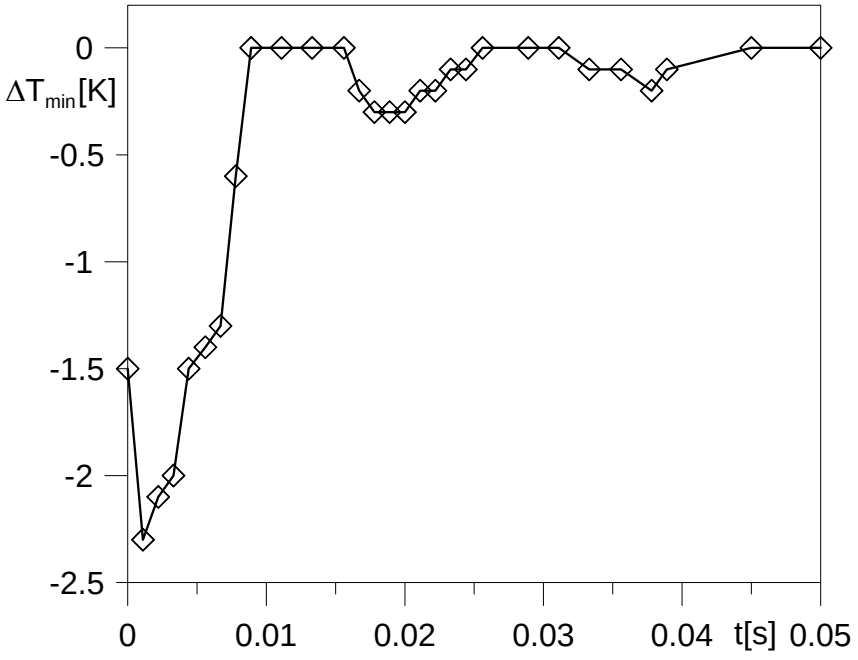

a) Minima ΔT

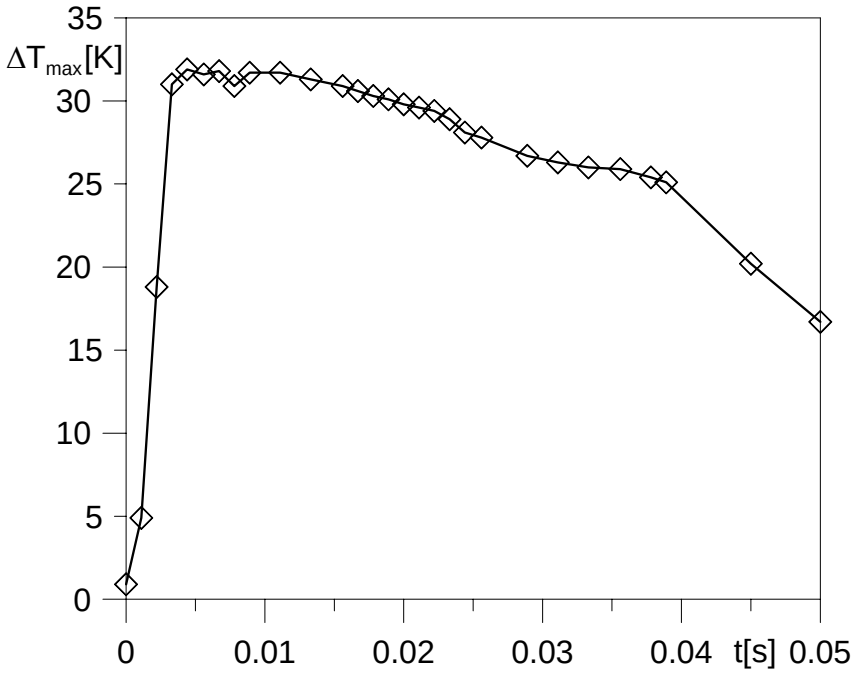

b) Maxima ΔT

Fig. 7 Minima and maxima ΔT values for impact energy of 12.3 J

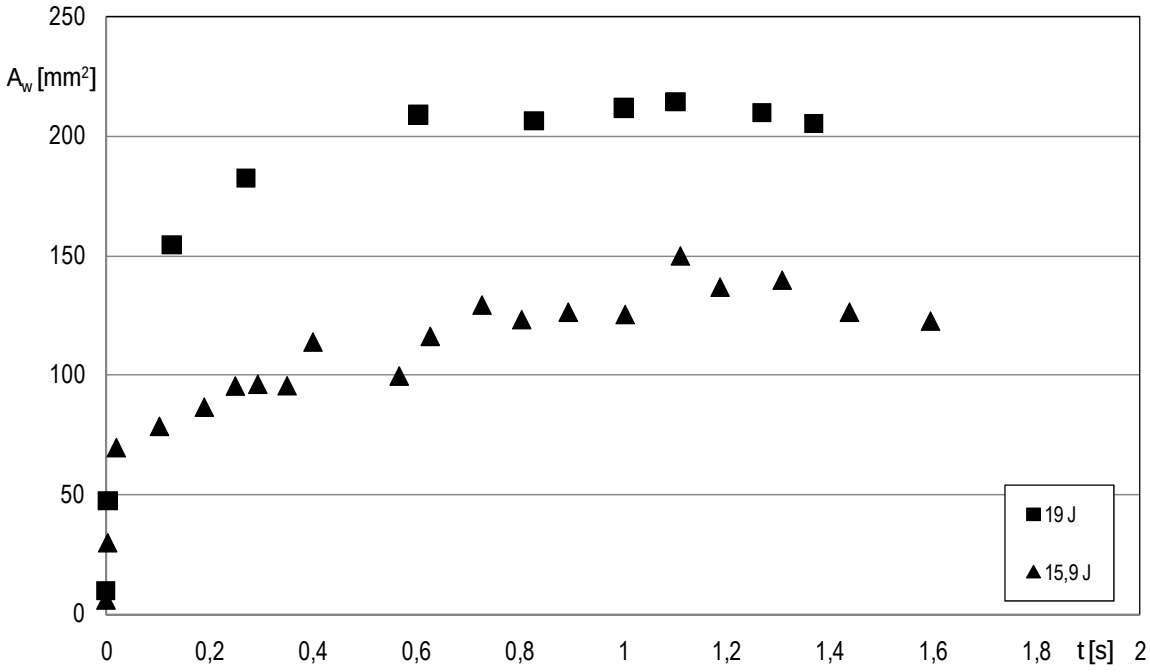

Fig. 8 Hot area variation with time

Non destructive evaluation

As already mentioned, each specimen was non-destructively inspected before and after impact with optical lock-in thermography. Several tests were carried out by varying the stimulation frequency *f*; to evaluate the material at different layers through the thickness according to the equation:

$$\mu = \sqrt{\frac{\alpha}{\pi f}} \qquad (2)$$

where μ is the thermal diffusion length, and α is the thermal diffusivity. In the classical optical lock-in method, for which both lamp and camera are located on the same side (Fig. 1), the thermal wave propagates inside the material and gets reflected when it reaches parts where the heat propagation parameters change (in-homogeneities). The reflected wave interferes with the surface wave producing an oscillating interference pattern, which can be measured in terms of amplitude, or phase angle, and, respectively, represented as amplitude, or phase, images. The depth range, for the amplitude image, is given by μ while the maximum depth *p*, which can be reached for the phase image, corresponds to 1.8μ [13-15].

Phase images of the specimen n. 13 taken at *f* = 0.14 Hz before and after impact are shown in Fig. 9(a-c). In particular, for a direct comparison, both images a) and b) before and after impact, are represented with the same phase range (0-0.2). In this way, the second image displays a white zone, which allows for a quick measure of the overall damaged area, but does not supply detailed information. Thus, the image in Fig. 9b is again represented in Fig. 9c with a wider phase angle range.

Going back to the first image (Fig. 9a), the non uniform phase angle, may be due to either non uniform density of the matrix, or presence of local porosity. Indeed, a material with a certain percentage of porosity was to be expected because of the manufacturing procedure, which was performed without vacuum bag. The white area in the second image (Fig. 9b), as always said, corresponds to the permanent damage caused by the impact. With reference to Fig. 9c, the smaller whiter central zone most probably indicates cracks in the

matrix and fibres rupture, while the adjacent larger area is characterized by delamination between fibres and matrix.

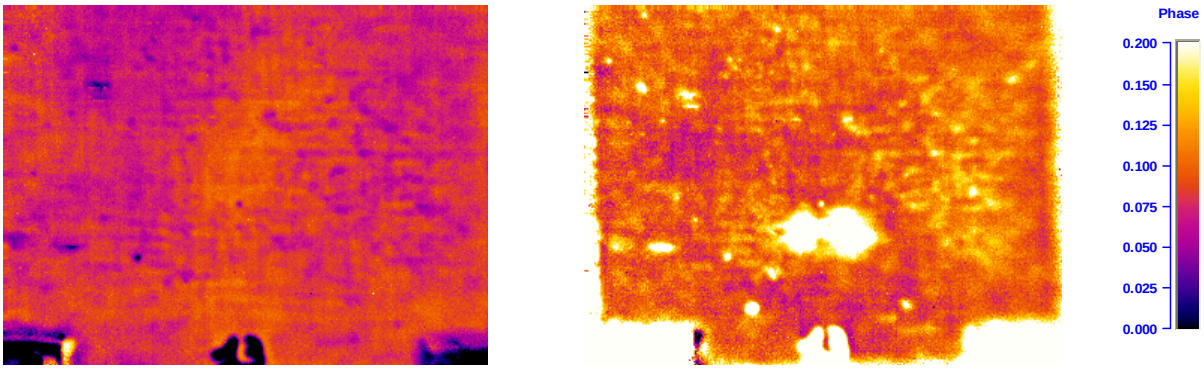

a) before impact

b) after impact at 16.6 J

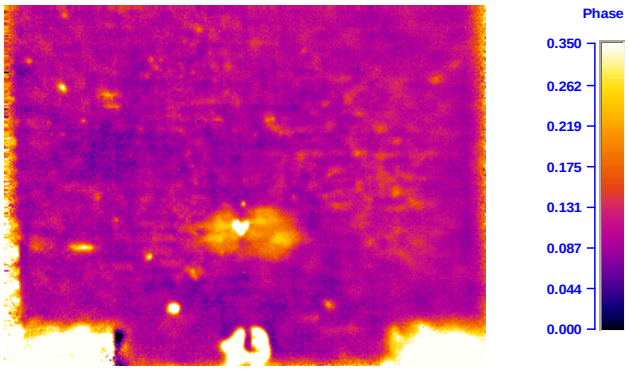

c) the same as in b with larger scale range

Fig. 9 Phase images of the specimen n.13 taken at f = 0.14 Hz

CONCLUSIONS

An infrared imaging system was used to analyze the response of an E-glass fibres reinforced polymer to low-velocity impact. Two types of investigations were carried out, one focused on the on-line monitoring during the impact and the other one focused on non destructive evaluation of the material before and after impact. The obtained results supply useful information for the material characterization and for estimation of the damage extension through the thickness and in plane at a given depth. In particular, the thermal images taken during impact allow for the assessment of both thermo-elastic and thermo plastic phases.

REFERENCES

[1] R.M. Jones, Mechanics of composite materials, Hemisphere Publishing Corporation, New York, 1975.
[2] D. Hull and T.W. Clyne, An introduction to composite materials, Cambridge University Press 1996.
[3] C. Soutis, *Progr. Aerosp. Sci.*, vol. 41, pp.143–151, 2005.
[4] C. Meola, G.M. Carlomagno, *Meas. Sci. Technol.* vol, 15, pp. 27-59, 2004.
[5] C. Meola, G.M. Carlomagno, *J. Adhesion Sci. Technol.* 20, pp. 589-632, 2006.
[6] G. Busse, Optoacoustic and photothermal material inspection techniques, *Appl. Opt.* vol. 21, pp. 107-110, 1982.

[7] J.L. Beaudoin, E. Merienne, R. Danjoux, M. Egee, in Proc. *SPIE* Infrared technology and applications*, vol.* 590, pp. 287-292, 1985.
[8] M.G. Beghi, C.E. Bottani, G. Caglioti, *Res Mech*. vol.19, pp. 365-379, 1986.
[9] J.M. Dulieu-Barton, T.R. Emery, S. Quinn and P.R. Cunningham, *Meas. Sci. Technol.*, vol. 17, pp. 1627- 1637, 2006.
[10] P.R. Cunningham, J.M. Dulieu-Barton, A.G. Dutton and R.A. Shenoi, *Key Eng. Mater*. Vol. 453, pp. 204-205, 2001.
[11] R.J.H. Paynter and A.G. Dutton, *Strain*, 39, pp. 73-78, 2003.
[12] C. Meola, G.M. Carlomagno, *Appl. Phys. D*, in press.
[13] A. Letho, J. Jaarinen, T. Tiusanen, M. Jokinen, M. Luukkala, *Electronic Lett.* vol. 17, pp. 364-365, 1981.
[14] C.A. Bennett, Jr., and R.R. Patty, *Appl. Opt.*, vol. *21*, pp. 49–54, 1982.
[15] G. Busse, *Appl. Phys. Lett.*, *35*, pp. 759–760, 1979.